| RESEARCH ARTICLE | OPEN ACCESS |

Damp-Heat–Induced Degradation of Lightweight Silicon Heterojunction Solar Modules With Different Transparent Conductive Oxide Layers

Kai Zhang[1,2] | Oleksandr Mashkov[3] | Muhammad Ainul Yaqin[1,2] | Bernd Doll[4,5] | Andreas Lambertz[1] | Karsten Bittkau[1] | Weiyuan Duan[1] | Ian Marius Peters[3] | Christoph J. Brabec[3,4] | Uwe Rau[1,2] | Kaining Ding[1]

[1]IEK-5 Photovoltaics, Forschungszentrum Jülich GmbH, Jülich, Germany | [2]Jülich Aachen Research Alliance (JARA-Energy) and Faculty of Electrical Engineering and Information Technology, RWTH Aachen University, Aachen, Germany | [3]Helmholtz-Institute Erlangen-Nürnberg for Renewable Energy (HI ERN, IEK-11), Forschungszentrum Jülich GmbH, Erlangen, Germany | [4]Institute of Materials for Electronics and Energy Technology (i-MEET), Friedrich-Alexander University Erlangen-Nürnberg, Erlangen, Germany | [5]LayTec AG, Berlin, Germany

Correspondence: Kai Zhang (k.zhang@fz-juelich.de) | Kaining Ding (k.ding@fz-juelich.de)

ABSTRACT

Lightweight photovoltaic applications are essential for diversifying the solar energy supply. This opens up vast new scenarios for solar modules and significantly boosts the capacity of renewable energy. To ensure high efficiency and stability of the solar modules, several challenges need to be overcome. Degradation due to elevated temperature and/or humidity is a critical concern for silicon heterojunction (SHJ) solar modules. Here, we investigated the stability and degradation mechanism of encapsulated cells with lightweight configurations where the cells are based on three different types of transparent-conductive oxide (TCO): indium tin oxide (ITO), aluminum-doped zinc oxide (AZO), and a combination of ITO/AZO/ITO under humid and thermal environmental conditions. A damp heat (DH) test at a temperature of 85°C and relative humidity (RH) of 85% was performed on lightweight modules for 1000 h. Our results show that AZO is the most susceptible to DH degradation. The AZO film was damaged by the combined effects of moisture ingress and delamination of the interconnection foil, resulting in a decrease in the conductivity of the AZO film, leading to a dramatic increase in R_s and a decrease in FF of the modules. Consequently, moisture has a greater chance of percolating through the damaged AZO layer into the a-Si:H passivation layer, causing passivation degradation, which leads to an increase in recombination, resulting in a decrease in V_{oc} of the modules. In particular, after capping the AZO film with an ITO film, the efficiency loss of the ITO/AZO/ITO module was significantly reduced. This suggests that the ITO film could be a promising protective capping layer for the AZO-based solar cells.

1 | Introduction

Global photovoltaic (PV) module manufacturing capacity increased to nearly 450 GW in 2022. According to the International Energy Agency (IEA), the global solar PV manufacturing capacity will nearly double by 2024, reaching almost 1 TW [1, 2]. In addition, integrated photovoltaics, such as building-integrated photovoltaics (BIPV) and vehicle-integrated photovoltaics (VIPV), have gained increasing attention in recent years, broadening the application scenario for PV technology. For these new applications, the combination of lightweight and high performance is becoming more important in the design of solar modules. Additionally,

lightweight modules can be installed on roofs with low load capacities, which is not possible for traditional glass modules [3]. Silicon heterojunction (SHJ) solar cells have been recognized as one of the most advanced technologies for improving solar power generation [4–7]. They can achieve high power conversion efficiencies (PCE) owing to their excellent surface passivation, which minimizes surface recombination, resulting in a higher open-circuit voltage (V_{oc}), and fill factor (*FF*) compared with other crystalline silicon (c-Si)–based technologies, such as aluminum back-surface field (Al-BSF) and passivated rear-emitter cell (PERC) [8]. The world record highest PCE of 26.81% for a large M6 (274.4 cm^2) both sides contacted SHJ cell was reported by LONGi in November 2022 [9]. In addition, the ideal passivated surfaces and the low temperature used during processing of the SHJ solar cell allow a thinner wafer to be used. SHJ solar cells are highly compatible with bifacial PV module designs and integrated PV applications owing to their symmetrical architecture.

Reducing the weight of modules and replacing glass and frame with alternative materials are emerging research topics in the PV industry. However, the stability and reliability of lightweight modules using the SHJ cell technology have not been widely investigated and reported. In addition to the various advantages mentioned above, there are some disadvantages associated with this technology. A major disadvantage compared with other solar cell concepts is the need for a transparent-conductive oxide (TCO) layer for lateral carrier transportation, such as indium tin oxide (ITO), which is widely used in industry. The power output of PV modules is affected by various environmental factors, such as irradiation, temperature, moisture ingress, wind and snow load, and soiling during long-term field operation. These environmental factors would degrade the modules and reduce their power output over time [10–14]. SHJ modules typically degrade at a rate of less than 1% per year in solar farms [15, 16]. The degradation is mainly in V_{oc}, with some increase in series resistance (R_s), which can differ from other technologies [17, 18]. Moreover, new failure modes can occur in field applications. The correct choice of encapsulants would protect the modules from environmental factors and weathering degradation, which significantly affects the performance and stability of the modules. In essence, this affects the cost and quality of the PV modules, and the appropriate combination of encapsulants and cell technology is critical to the longevity of the modules. Damp heat (DH) test generates a large amount of water vapor on the surface of the PV modules and drives it into the module. Elevated temperatures can correspondingly accelerate the water vapor penetration process, which can lead to various degradations such as corrosion, delamination, or discoloration [19–24]. This damp-heat–induced degradation (DHID) is typically accompanied by severe reductions in module performance [25]. Regarding the long-term reliability of the SHJ cells and modules, the stability of the TCO film is always a hot topic for the PV community. TCO is generally highly susceptible to degradation due to water vapor ingress and acid corrosion [26, 27], which requires better encapsulation to enhance the lifetime of the SHJ module. Another potential bottleneck in the large-scale development and production of SHJ solar cell technology is the use of rare elements and materials, such as indium (In). ITO is widely used in the electronics industry and as a TCO layer in PV industry [28]. To address this issue, intensive efforts have been made in recent years to overcome this potential limitation. Potential solutions

being investigated include indium-free TCO, indium-less TCO, and TCO-free concepts [29, 30]. The aim of indium-free TCO is to get rid of indium completely [31, 32]. One possible and ongoing research is to replace ITO with aluminum-doped zinc oxide (AZO). However, the pure AZO film has lower carrier mobility and higher resistivity [33] and is more susceptible to water vapor corrosion. This results in a reported loss of conductivity [34]. AZO grows in a polycrystalline structure that favors rapid penetration of water molecules into the crystal boundaries, leading to degradation of the electrical properties of the material [35]. Therefore, in order to improve the electrical properties of AZO and to enhance the damp heat stability of the AZO film, different capping layers have been introduced and investigated at the cell level, such as Al_2O_3, SiO_x, and SiN_x. Adachi et al. reported that a SiO_x capping layer on the ITO layer improved the damp heat stability of SHJ solar cells [26]. Morales-Vilches et al. reported that the damp heat stability of cells with AZO front TCO was improved when capped with SiO_2; SiO_2 capping layer hindered the moisture-induced degradation of AZO at the grain boundaries [36]. Indium-less TCO mainly consist of, for example, AZO, which is capped by a very thin ITO layer, possibly also an ITO seed layer [33]. In our previous study [33], a 10-nm ITO layer was introduced between the AZO and n-type doping hydrogenated amorphous silicon [a-Si:H(n)] as a seed layer to reduce the contact resistance of the AZO with a-Si:H(n), and a 10-nm ITO layer was introduced on top of the AZO as a capping layer. The device with ITO/AZO/ITO as front TCO and pure AZO as rear TCO was successfully fabricated with high efficiency and reduced the indium consumption by 85% [33].

To thoroughly investigate the damp heat stability of SHJ cells based on three types of TCO films (ITO/AZO/ITO, AZO, and ITO) within a lightweight module architecture, the modules were fabricated and tested accordingly. This work reports the damp heat stability of an AZO film–based SHJ module with a lightweight configuration. The degradation mechanism was explicitly analyzed. The results of this work could provide valuable reference information for the development of damp heat stable AZO-based lightweight SHJ solar modules.

2 | Method and Approach

2.1 | Preparation of Tested Samples

2.1.1 | The Solar Cells Used for Fabrication of Modules

All solar modules were prepared as 200 mm × 200 mm single-cell minimodule samples using M2+ (245.72 cm^2) bifacial monocrystalline busbar-free n-type rear-junction SHJ solar cells with three types of TCO layers. Figure 1 shows the structures of the SHJ cells with different TCO layers. ITO was used as a reference. AZO and capped ITO/AZO/ITO were used as alternative TCO. The first one used 70-nm ITO as the front and rear TCO layers. The second one used 70-nm AZO as the front and rear TCO layers. The third one used a triple-layer structure ITO (10 nm)/AZO (50 nm)/ITO (10 nm) stack as the front TCO layer and 70-nm AZO as the rear TCO layer. Here, the ITO on top of the AZO acts as a capping layer, whereas the ITO on the bottom of the AZO acts as a seed layer. The fabrication process of the solar cells was done at our SHJ solar cell baseline [37]. The
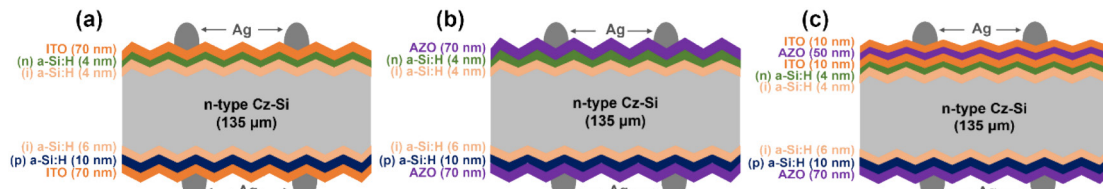
FIGURE 1 | Schematic cross-section of SHJ solar cells with different TCO layers: (a) ITO at the front and rear sides, (b) AZO at the front and rear sides, and (c) ITO/AZO/ITO at the front and AZO at the rear side.
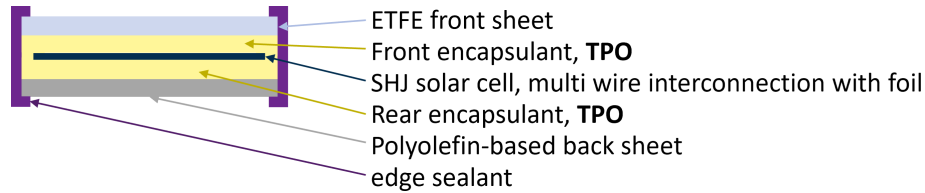

FIGURE 2 | Schematic cross-section of SHJ solar module.

parameter optimization of the films and devices regarding the counterbalance between optical and electrical properties was already reported from our previous work [33].

2.1.2 | Choice of the Encapsulants

Two types of encapsulants were introduced when we designed and fabricated modules. One was EPE, which is a co-extruded ethylene vinyl acetate (EVA) and polyolefin elastomer (POE), with a stack structure of EVA/POE/EVA. The other was thermoplastic polyolefin (TPO). The specifications of the encapsulants are shown in Table S1 and the optical properties of the encapsulants are shown in Figure S1. We made a comparison between the EPE encapsulated module and the TPO encapsulated module in the DH test at 85°C and 85% relative humidity (RH) conditions. Table S2 lists the configurations of the TPO/TPO encapsulated and EPE/TPO encapsulated module samples. The variations in the electrical parameters from cell to module (CTM) are shown in Figure S2. The optical properties of the modules were characterized by the external quantum efficiency (*EQE*), as shown in Figure S3. The DH results are shown in Figures S4–S7. The 1000-h DH results show that the TPO encapsulated module is more stable than the EPE encapsulated module. Therefore, the TPO was used as the front and rear encapsulant to fabricate the modules based on cells with different TCO films in order to minimize the impact of the encapsulant materials on the cells during the DH test.

2.1.3 | Fabrication of the Modules

Figure 2 shows the schematic cross-section of the single-cell minimodules. In terms of module encapsulation, poly-ethene-co-tetrafluoroethene (ETFE) was used as the front cover material, which has a higher transmittance than glass commonly used in the PV industry; see Figure S8. The specification of the ETFE is shown in Table S3. The solar cell is located between the front and rear encapsulants (TPO). The cells were connected using multi-wire interconnection technology consisting of 18 coated copper wires with polyolefin as the carrier foil (interconnection foil).

TABLE 1 | Configurations of the test module samples.

No.	Front sheet	Encapsulants (front/rear)	Cell with different TCO layers	Back sheet
1	ETFE	TPO/TPO	ITO	Px-bs
2	ETFE	TPO/TPO	AZO	Px-bs
3	ETFE	TPO/TPO	ITO/AZO/ITO	Px-bs

Sn-Pb-coated copper ribbons (5 mm wide, 0.2 mm thick) were used as connectors. A polyolefin-based foil with fluorine-free coating was used as the back sheet (hereafter referred to as Px-bs). The specification of the Px-bs is shown in Table S3.

After all the foils had been layered, the vacuum lamination process was carried out at 125°C and 750 mbar for 14 min. All the modules were laminated using an *SM Innotech* membrane laminator. After lamination, the edges of all modules were sealed with acrylic foam adhesive tape to prevent moisture from ingress into the module. The specification of the edge sealant is shown in Table S4. Table 1 lists the configurations of the test module samples. Two identical modules were fabricated for each configuration in subsequent tests.

Prior to making the cell into the module, the electrical properties (electroluminescence [EL] images and current–voltage [*I-V*] characteristics) of the cells were characterized. After lamination, the module samples were characterized by visual inspection, optical properties (external quantum efficiency [*EQE*] and reflectance), and electrical properties (EL, photoluminescence [PL] images, and *I-V* characteristics).

2.2 | Damp Heat Accelerated Aging Test

After the module samples were prepared, the modules were subjected to a cumulative 1000 h of damp heat test at 85°C and 85%

RH in a climate chamber according to IEC 61215: 2021 [38]. The *I-V* characteristics and EL images of modules were periodically characterized at 200-h intervals during the DH test to track the aging process.

2.3 | Characterization of the Samples

The *I-V* characteristics of the tested module samples were characterized using a flash system (Spi-Sun Simulator 4600SLP) under standard test conditions (25°C, AM 1.5G, 1000 W/m^2): (i) before (initial state), (ii) at intermediate assessment points (every 200 h of the DH test), and (iii) at the final state (after 1000 h of the DH test). Open-circuit voltage (V_{oc}), short-circuit current density (J_{sc}), series resistance (R_s), shunt/parallel resistance (R_{sh}), fill factor (*FF*), power at maximum power point (MPP) (P_{MPP}), voltage at MPP (V_{MPP}), and current at MPP (I_{MPP}) were determined.

EQE and integral reflectance were measured using monochromatic illumination and an integrating sphere. The measurements were performed using a LOANA solar cell analysis system from PV-Tools.

EL imaging was used to identify electrical homogeneity and visualize the defects that affect module performance [39–42]. Electrical inhomogeneities caused by cell cracks, corrosion, or contact failure can be detected [31]. However, the evaluation of EL images alone risks convoluting material quality with electrical contact issues, whereas PL imaging optically excites all materials regardless of electrical connectivity. The combination

of both approaches can provide important insight into module characteristics and causes of degradation [43].

3 | Results and Discussion

3.1 | CTM Analysis

The electrical properties of the module were characterized using a flash system. The variations in the electrical parameters from CTM are shown in Figure 3. The efficiency loss from the cell to the module is approximately 2% (abs.). This was mainly attributed to the loss of *FF* and J_{sc}. The *FF* loss is mainly due to the increase in R_s after cell interconnection. The J_{sc} loss is mainly due to the light reflection from the front surface and light absorption by the front sheet and encapsulant materials. The optical properties of the modules were characterized by the *EQE*. The *EQE* of the modules with three types of TCO layers are shown in Figure 4. The ITO module shows a slightly higher *EQE* than the AZO and ITO/AZO/ITO modules. The slightly lower *EQE* of the AZO module can be ascribed to higher absorption of the AZO layer [33].

3.2 | DHID on Different TCO Films–Based SHJ Lightweight Modules

Figure 5 shows the time evolution of the degradation of the electrical properties of the SHJ modules with different TCO films at fixed time intervals during the DH test. Each value was normalized to its initial value (before the DH test). The raw data and *I-V*
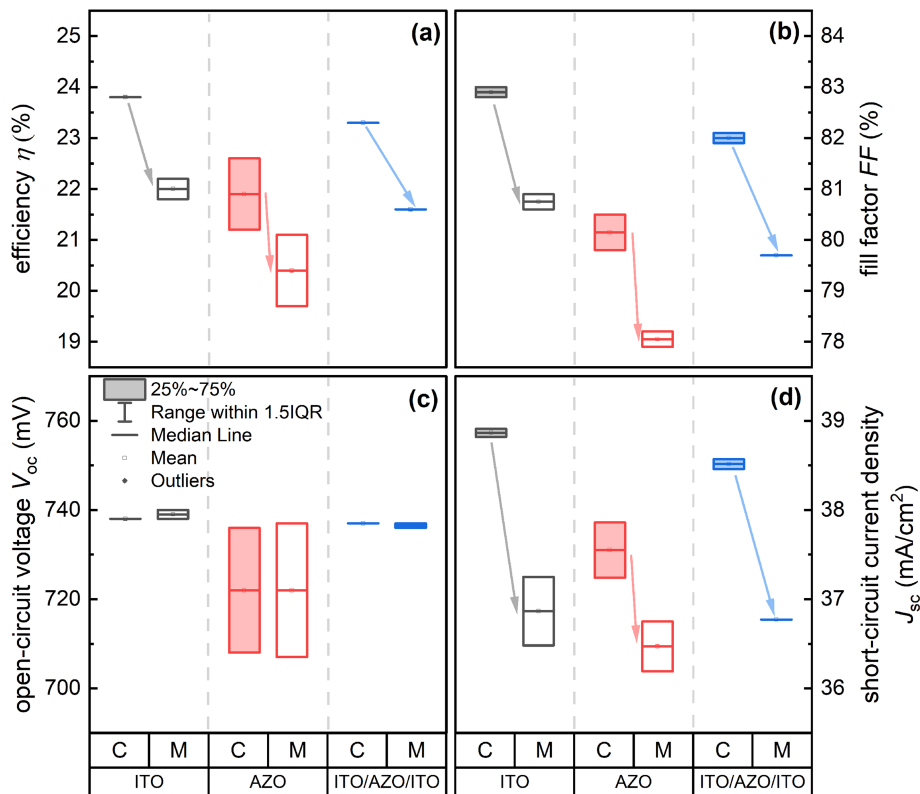

FIGURE 3 | CTM analysis of (a) efficiency (*η*), (b) fill factor (*FF*), (c) open-circuit voltage (V_{oc}), (d) short-circuit current density (J_{sc}). C stands for cell and M stands for module.
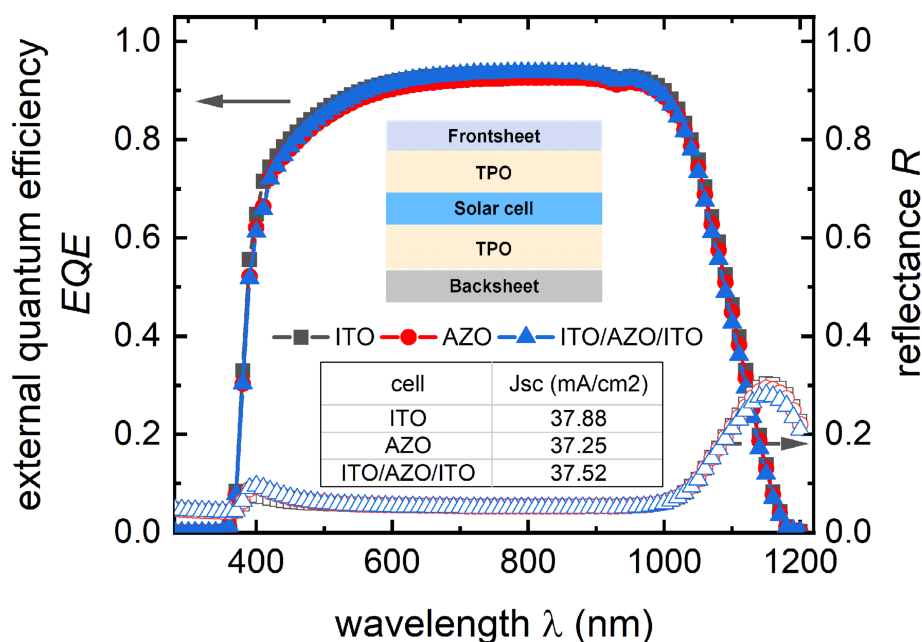
FIGURE 4 | *EQE* (solid symbols) and reflectance (hollow symbols) of the modules with three types of TCO layers. A schematic of the single-cell minimodule sample is shown in the inset.

curves are shown in Figure S9. The AZO film module was found to degrade by 58.57% in efficiency after 1000 h of DH test, which is due to the losses in *FF* (44.24%) and J_{sc} (23.47%). The *FF* degradation is primarily caused by the dramatic increase in R_s [17]. A significant increase in R_s could be attributed to an increase in sheet resistance of the AZO front electrode or deterioration of the AZO/a-Si interface. It is assumed that this degradation is due to the effect of the humidity on the AZO film, which causes a decrease in conductivity when the sample is exposed to damp heat conditions, as observed by Greiner et al. [34, 35]. AZO grows in a crystalline structure that favors a rapid penetration of the water molecules into the crystal boundaries, leading to a degradation of the electrical properties of the material [36]. D. Greiner et al. also reported that the non-encapsulated modules after damp heat exposure show an increased series resistance, which is mostly attributed to the increase in the lateral sheet resistance of the transparent AZO front contact [34]. In general, AZO cells with glass/glass encapsulation are able to show stable performance in the DH test, as shown by the red star in Figure 5. Regarding the ITO/AZO/ITO module samples, a small decrease in *FF* is observed compared with the AZO samples, indicating the effectiveness of the ITO as a protective capping layer.

From the EL images in Figure 6b, two different defects can be clearly identified. The circular dark area (white dashed line) in the center of the AZO film module as prepared before the DH test was caused by sputter damage on a-Si:H due to ion bombardment [44] during the AZO deposition process, as reported in our previous study [33]. This circular dark area became darker with prolonged DH test, indicating that the passivation damage of the cell increased and higher carrier recombination led to a decrease in module V_{oc}. This indicates that the passivation of the cell was gradually further degraded by moisture ingress through the AZO layer with DH exposure time. In order to determine this, the AZO film was deposited on glass and subjected to a 600-h DH test under the same conditions as the

tested modules. The morphological changes (becoming more porous) observed in the AZO films by scanning electron microscopy (SEM) after 600 h of the DH test indicate that water vapor molecules diffuse and percolate through the AZO films [45]. The SEM images are shown in Figure 7. However, the sputter damage was not observed when a 10-nm ITO seed layer was introduced between the AZO and n-type a-Si:H [33]. In contrast, the rectangular dark area (red dashed line) defects formed in the DH test were due to the degradation of the AZO layer by moisture ingress. This failure mode was further confirmed by PL measurements under open-circuit conditions. The rectangular dark area appeared only in the EL image and not in the PL image, suggesting that this defect was due to electrical degradation of the AZO film rather than passivation degradation. The cracks in the modules shown in the PL images were caused by the transport of the modules. The difference between the PL and EL patterns indicates a local increase in R_s with long-term field exposure [46]. The lower EL intensity is caused by drops in local junction voltage due to higher R_s, whereas the open-circuit PL is dominated by semiconductor quality and local defect configuration, which should not be affected by contact issues causing an increase in R_s [18]. Thus, the rectangular dark area defects in EL indicate that the carriers cannot be properly transported through the deteriorated AZO film. Therefore, we can conclude that the electrical properties of the AZO film have changed after 1000 h of the DH test, resulting in an increase in the resistivity of the AZO films, leading to a dramatic increase in R_s and a corresponding decrease in *FF*. One hypothesis for the cause of this rectangular dark area defect is that the adhesion of the AZO layer to the interconnection foil is weaker than that of ITO. Moisture ingress caused the interconnection foil to delaminate from the AZO layer during the DH test, thereby damaging the AZO layer. From the visual inspection of the module as shown in Figure S10, we found that a severe delamination occurred along the wires on the AZO modules. We can clearly see the voids in this area. This is more likely to be the interconnection
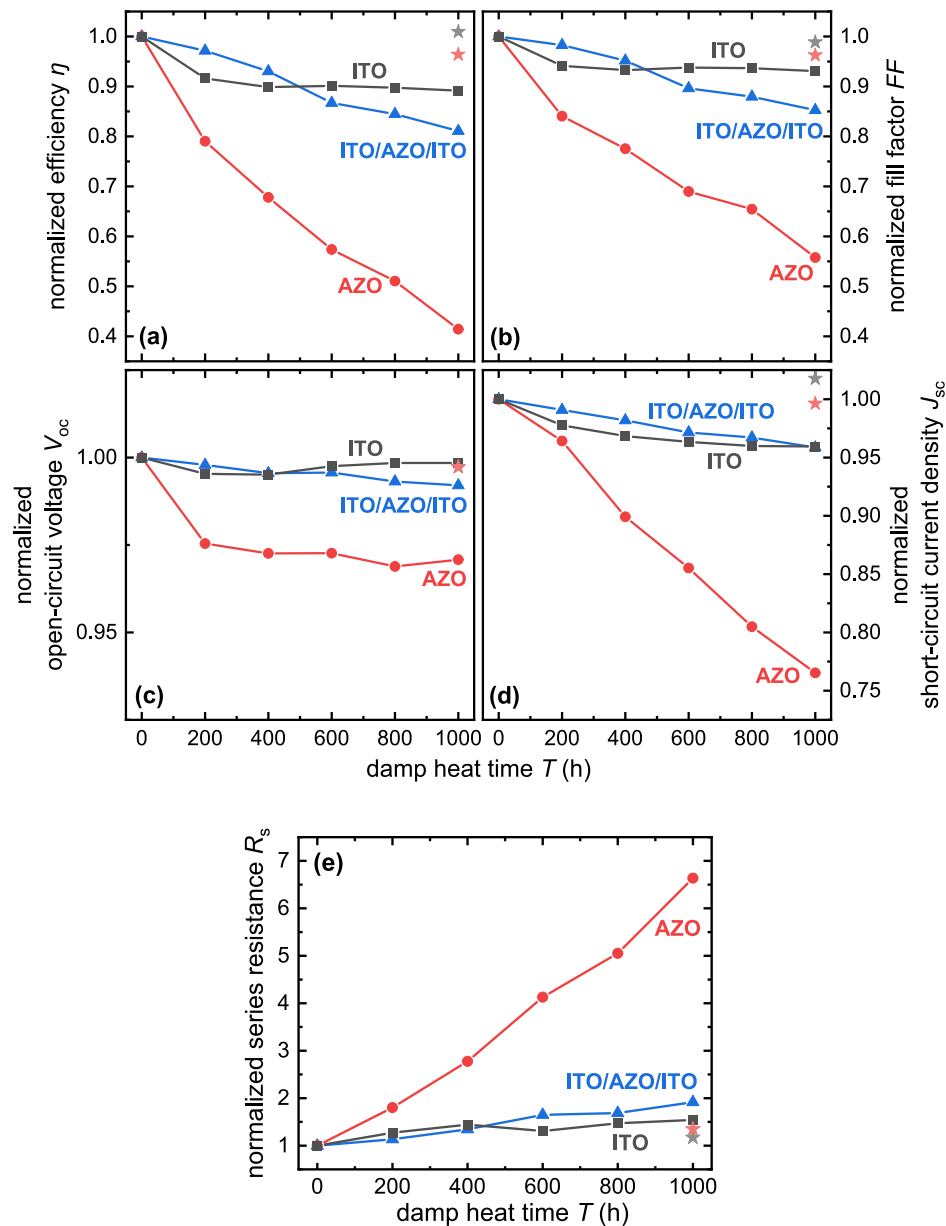
FIGURE 5 | Normalized values of (a) efficiency (η), (b) fill factor (FF), (c) open-circuit voltage (V_{oc}), (d) short-circuit current (J_{sc}), and (e) series resistance (R_s) as a function of damp heat time for modules with different TCO. The red star shows the degradation of a glass/glass encapsulated AZO module after 1000 h of the DH test. The gray star shows the degradation of a glass/glass encapsulated ITO module after 1000 h of the DH test.

foil delaminating from the AZO layer than the AZO delaminating from the wafer. However, this delamination defect is very small in the ITO module samples. Another hypothesis is that the AZO layer was degraded by substances released from the interconnection foil that reacted with the water molecules. Both hypothesized degradation modes were highly correlated with the interconnection foil. Therefore, an additional experiment was conducted to validate these hypotheses. We manually removed half of the interconnection foil, leaving only the wires, and left the other half intact, and then performed interconnection and lamination. The details are shown in Figure S11. The EL images taken after 1000 h of the DH test show that the rectangular dark area is not visible at the sample position where the interconnection foil has been removed. It is thus identified that the rectangular dark area defect in the AZO module samples was caused by the interconnection foil. In contrast, the rectangular

dark area in the module with ITO/AZO/ITO as the front TCO layer is not as dark as that in the module with pure AZO as the front TCO layer. As shown in Figure 5a, the efficiency loss of the ITO/AZO/ITO module is significantly lower than that of the AZO module. The DH stability of the AZO film was found to be further improved after capping with ITO as a protective layer. However, the 10-nm-thick ITO capping layer did not provide sufficient adhesion to the interconnection foil. Delamination defects could also be observed in the ITO/AZO/ITO module but were not severe compared with the AZO module, as shown in Figure S10.

In contrast, the ITO module showed a diametrically opposite phenomenon to that of the AZO module. The EL images of the ITO module show a higher intensity in the rectangular area where the interconnection foil is located (as indicated by the
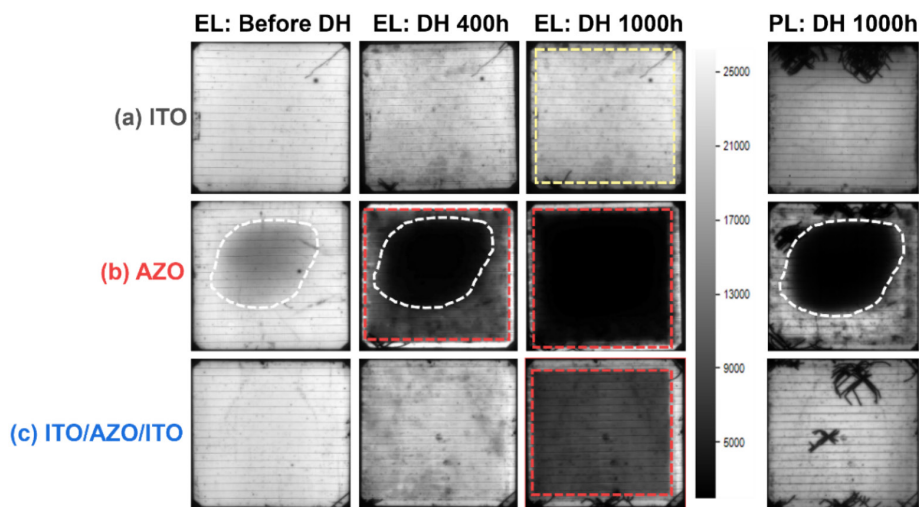
FIGURE 6 | EL and PL images of the (a) ITO, (b) AZO, and (c) ITO/AZO/ITO film–based SHJ modules before and after the DH test. The severe cracking of the module shown in the PL images was due to the transport after the *I-V* and EL measurements.
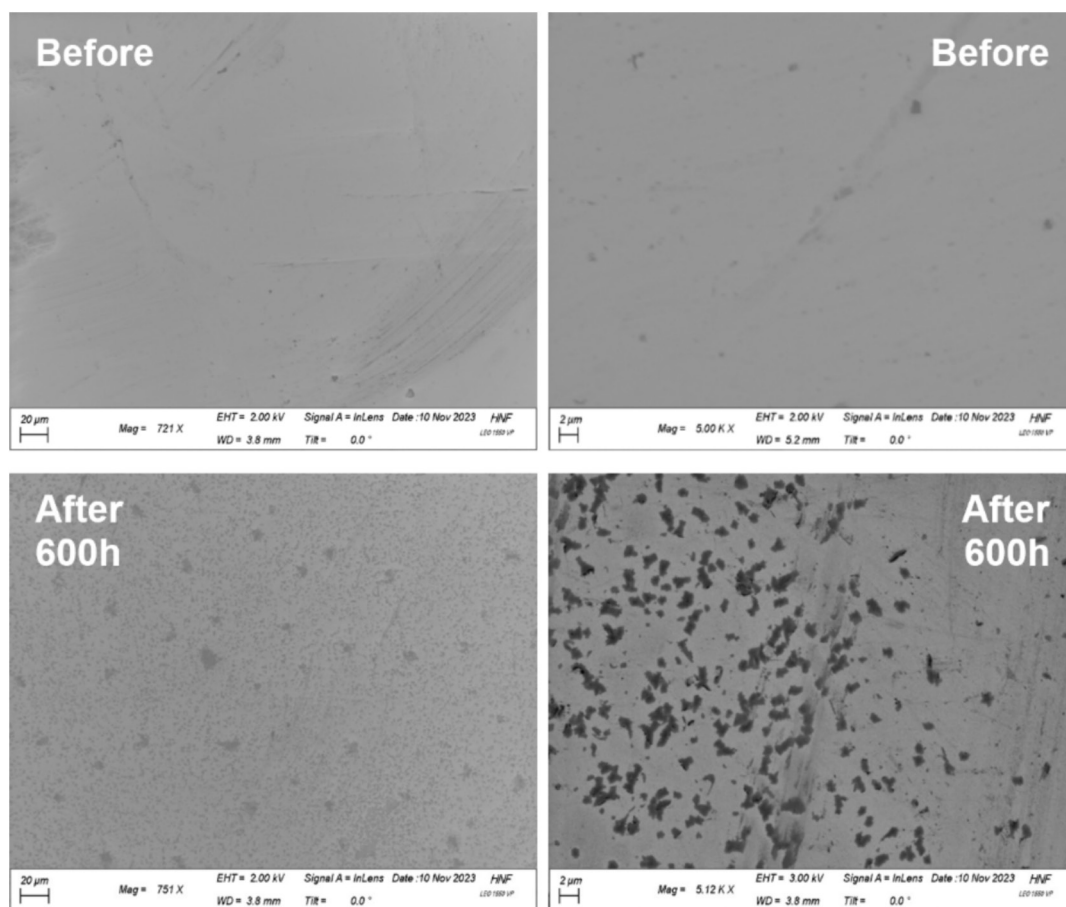

FIGURE 7 | Scanning electron microscopy (SEM) images of the surface morphology of the AZO films before and after 600 h of the DH test. The AZO film was deposited on corning glass using the same sputtering process as that used for cell fabrication.

yellow dashed line in Figure 6a) than at the edges of the module. This is more like an edge effect. The ITO film modules show almost no delamination. These indicate that the interconnection foil has better adhesion to the ITO layer than to the AZO layer. Therefore, the interconnection foil can be considered an additional encapsulation foil to provide additional protection to the ITO layer against moisture ingress. As a result, the edges of the module where there is no interconnection foil are more susceptible to moisture ingress. Therefore, we found that the central area of the ITO module, where there is an interconnection foil, showed a higher EL intensity than the areas where there is no interconnection foil in the EL images.
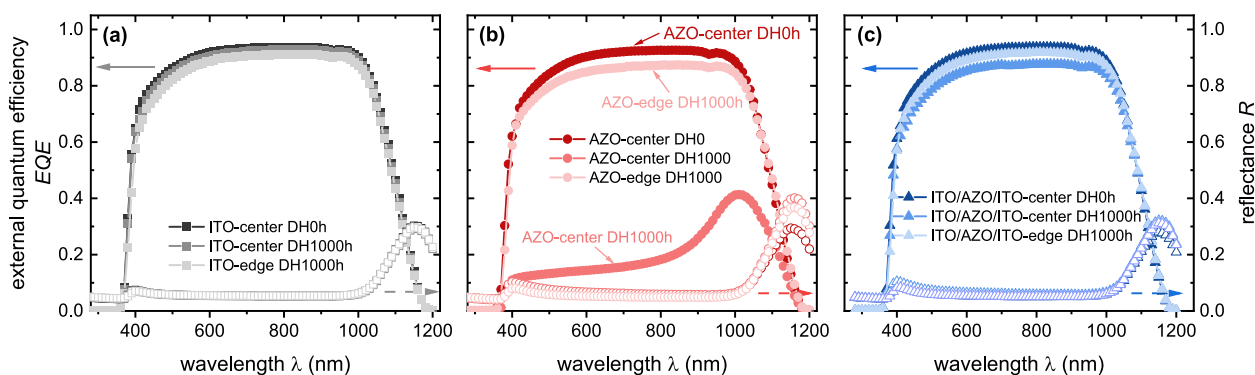
FIGURE 8 | *EQE* (solid symbols) and reflectance (hollow symbols) of (a) ITO, (b) AZO, (c) ITO/AZO/ITO film–based SHJ modules before and after 1000 h of the DH test. The measurement was conducted at different positions of the modules; the center indicates that the light spot is in the middle of the solar cell, and the edge indicates that the light spot is close to the edge of the solar cell. The location of the light spot is shown in Figure S12.

3.3 | Interpretation of Degradation Mechanisms

Based on the above analyses, we interpret the degradation mechanisms of the AZO film module as follows: (1) The delamination of the interconnection foil with the AZO film is due to moisture ingress and poor adhesion of the AZO film to the interconnection foil. (2) Delamination allows moisture to easily penetrate the AZO film. The AZO film was damaged by the combined effects of delamination and moisture ingress, causing vacancies in the AZO layer and resulting in a decrease in the conductivity of the AZO film, leading to a dramatic increase in R_s and a corresponding decrease in the *FF* of the AZO modules. The dramatic increase in R_s leads to a decrease in carrier collection efficiency, resulting in a significant decrease in J_{sc}. (3) Consequently, moisture has a greater chance of percolating through the damaged AZO layer into the a-Si:H passivation layer, causing passivation degradation, which leads to an increase in recombination, resulting in a decrease in V_{oc} of the AZO modules. The above phenomena occurred primarily in the area where the interconnection foil is located. This also explains why the *EQE* intensity (shown in Figure 8b) decreased significantly at the center rather than at the edges of the module after 1000 h of the DH test.

It is currently not easy to quantify the extent of moisture penetration through the encapsulation foil into the TCO and passivation layers. Nevertheless, this study clearly elucidates the degradation behavior of the AZO-based lightweight SHJ modules and demonstrates the importance of the capping layer to prevent moisture diffusion in AZO-based SHJ solar cells and modules. In addition, other possible capping layers should be investigated to further improve their ability to prevent moisture diffusion and to provide strong adhesion to the interconnection foil.

In addition, some small cracks appeared on the edges of the module during the DH process. This was due to the softening and slight bending of the edges of the modules during the DH process at temperatures up to 85°C, as the modules were placed vertically in the climate chamber. Therefore, we believe that the thermal expansion and shrinkage of the polymer front sheet are more severe than those of the glass during the DH process and would be even more severe during the thermal cycling (TC) process. This will be further investigated in our future studies.

4 | Conclusions

In this study, we investigated the DH stability of the special lightweight mini-SHJ solar modules based on three TCO films through an accelerated DH aging test. A comparison of the three types of TCO film modules shows that AZO is the most susceptible to damp heat degradation. The efficiency of the AZO module decreased by 58.57%, which was dominated by a large increase in R_s and significant decrease in *FF*. The poor adhesion of the AZO layer to the interconnection foil accelerates the penetration of moisture, leading to severe degradation of the AZO layer. In addition, moisture penetrates through the AZO layer and damages the passivation layer. Therefore, it is important to consider the adhesion of the polymer interconnection foil to the AZO layer to ensure that the module has a sufficient lifetime and stability for large-scale applications. Notably, the efficiency loss of the ITO/AZO/ITO module was effectively reduced to 18.92% after capping the AZO with an ITO layer, which suggests that the ITO layer has potential to enhance the moisture resistance and improve the DH stability, and thus is expected to be a promising protective capping layer for AZO-based SHJ solar cells. This study focused on a very specific type of lightweight module. The results of this study can provide valuable reference information for the development of damp heat stable AZO-based lightweight SHJ solar modules.

Conflicts of Interest

The authors declare no conflicts of interest.

Data Availability Statement

The data supporting the findings of this study are available from the corresponding author upon reasonable request.

References

1. IEA, "Trends in photovoltaic applications 2023-report IEA PVPS T1-43: 2023," (2023).

2. "Renewable Energy Market Update Outlook for 2023 and 2024."

3. A. C. Martins, V. Chapuis, A. Virtuani, H. Y. Li, L. E. Perret-Aebi, and C. Ballif, "Thermo-Mechanical Stability of Lightweight Glass-Free Photovoltaic Modules Based on a Composite Substrate," *Solar Energy Materials & Solar Cells* 187 (2018): 82–90, https://doi.org/10.1016/j.solmat.2018.07.015.

4. C. Ballif, S. D. Wolf, A. Descoeudres, et al., "Amorphous Silicon/Crystalline Silicon Heterojunction Solar Cells," *Semiconductors & Semimetals* 90, no. 12 (2014): 73–120, https://doi.org/10.1016/B978-0-12-388417-6.00003-9.

5. S. D. Wolf, A. Descoeudres, Z. C. Holman, et al., "High-Efficiency Silicon Heterojunction Solar Cells: A Review," *Green* 2 (2012): 7–24, https://doi.org/10.1515/green-2011-0018.

6. W. G. J. H. M. Sark, L. Korte, and F. Roca, *Physics and Technology of Amorphous-Crystalline Heterostructure Silicon Solar Cells* (Berlin: Springe-Verlag, 2011), https://doi.org/10.1007/978-3-642-22275-7.

7. A. Louwen, V. W. Sark, and R. Schropp, "A Cost Roadmap for Silicon Heterojunction Solar Cells," *Solar Energy Materials & Solar Cells* 147 (2016): 295–314, https://doi.org/10.1016/j.solmat.2015.12.026.

8. C. Ballif, F. J. Haug, M. Boccard, P. J. Verlinden, and G. Hahn, "Status and Perspectives of Crystalline Silicon Photovoltaics in Research and Industry," *Nature Reviews Materials* 7 (2022): 597–616, https://doi.org/10.1038/s41578-022-00423-2.

9. H. Lin, M. Yang, X. Ru, et al., "Silicon Heterojunction Solar Cells With up to 26.81% Efficiency Achieved by Electrically Optimized Nanocrystalline-Silicon Hole Contact Layers," *Nature Energy* 8 (2023): 789–799, https://doi.org/10.1038/s41560-023-01255-2.

10. H. Park, J. S. Jeong, E. Shin, and S. Y. J. Kim, "A Reliability Study of Silicon Heterojunction Photovoltaic Modules Exposed to Damp Heat Testing," *Microelectronic Engineering* 216 (2019): 111081, https://doi.org/10.1016/j.mee.2019.111081.

11. A. Ndiaye, C. M. F. Kébé, A. Charki, V. Sambou, and P. A. Ndiaye, "Photovoltaic Platform for Investigating PV Module Degradation," *Energy Procedia* 74 (2015): 1370–1380, https://doi.org/10.1016/j.egypro.2015.07.783.

12. T. Ishii and A. Masuda, "Annual Degradation Rates of Recent Crystalline Silicon Photovoltaic Modules," *Progress in Photovoltaics: Research and Applications* 25, no. 12 (2017): 953–967, https://doi.org/10.1002/pip.2903.

13. E. L. Meyer and E. E. V. Dyk, "Assessing the Reliability and Degradation of Photovoltaic Module Performance Parameters," *IEEE Transactions on Reliability* 53, no. 1 (2004): 83–92, https://doi.org/10.1109/TR.2004.824831.

14. A. Pozza and T. Sample, "Crystalline Silicon PV Module Degradation After 20 years of Field Exposure Studied by Electrical Tests, Electroluminescence, and LBIC," *Progress in Photovoltaics: Research and Applications* 24, no. 3 (2016): 368–378, https://doi.org/10.1002/pip.2717.

15. D. C. Jordan and S. R. Kurtz, "Photovoltaic Degradation Rates—An Analytical Review," *Progress in Photovoltaics: Research and Applications* 21, no. 1 (2013): 12–29, https://doi.org/10.1002/pip.1182.

16. D. C. Jordan, T. J. Silverman, J. H. Wohlgemuth, S. R. Kurtz, and K. T. VanSant, "Photovoltaic Failure and Degradation Modes," *Progress in Photovoltaics: Research and Applications* 25, no. 4 (2017): 318–326, https://doi.org/10.1002/pip.2866.

17. D. C. Jordan, C. Deline, S. Johnston, et al., "Silicon Heterojunction System Field Performance," *IEEE Journal of Photovoltaics* 8, no. 1 (2018): 177–182, https://doi.org/10.1109/JPHOTOV.2017.2765680.

18. C. S. Jiang, D. B. Sulas-Kern, H. R. Moutinho, et al., "Local Resistance Measurement for Degradation of c-Si Heterojunction with Intrinsic Thin Layer (HIT) Solar Modules," in *2020 IEEE 47th Photovoltaic Specialists Conference (PVSC)*, (Calgary, AB, Canada: IEEE, 2020): 1697–1701, https://doi.org/10.1109/PVSC45281.2020.9301011.

19. J. Zhu, M. Koehl, S. Hoffmann, et al., "Changes of Solar Cell Parameters During Damp-Heat Exposure," *Progress in Photovoltaics: Research and Applications* 24, no. 10 (2016): 1346–1358, https://doi.org/10.1002/pip.2793.

20. J. H. Wohlgemuth, D. W. Cunningham, A. M. Nguyen, et al., "Long term reliability of PV modules. In: 20th European Photovoltaic Solar Energy Conference and Exhibition, Barcelona, Spain," EU PVSEC Proceedings; 2005:1942–1946.

21. P. Hacke, K. Terwilliger, S. Glick, et al., "Test-to-Failure of Crystalline Silicon Modules," in *2010 35th IEEE Photovoltaic Specialists Conference*, (Honolulu, HI, USA: IEEE, 2010): 244–250, https://doi.org/10.1109/PVSC.2010.5614472.

22. M. A. Quintana, D. L. King, T. J. McMahon, et al., "Commonly Observed Degradation in Field-Aged Photovoltaic Modules," in *2002 Conference Record of the Twenty-Ninth IEEE Photovoltaic Specialists Conference*, (New Orleans, LA, USA: IEEE, 2002): 1436–1439, https://doi.org/10.1109/PVSC.2002.1190879.

23. G. J. Jorgensen, K. M. Terwilliger, J. A. Delcueto, et al., "Moisture Transport, Adhesion, and Corrosion Protection of PV Module Packaging Materials," *Solar Energy Materials & Solar Cells* 90, no. 16 (2006): 2739–2775, https://doi.org/10.1016/j.solmat.2006.04.003.

24. Y. Voronko, G. C. Eder, M. Knausz, G. Oreski, T. Koch, and K. A. Berger, "Correlation of the Loss in Photovoltaic Module Performance With the Ageing Behaviour of the Backsheets Used," *Progress in Photovoltaics: Research and Applications* 23, no. 11 (2015): 1501–1515, https://doi.org/10.1002/pip.2580.

25. C. Peike, S. Hoffmann, P. Hülsmann, et al., "Origin of Damp-Heat Induced Cell Degradation," *Solar Energy Materials & Solar Cells* 116 (2013): 49–54, https://doi.org/10.1016/j.solmat.2013.03.022.

26. D. Adachi, T. Terashita, T. Uto, J. L. Hernández, and K. Yamamoto, "Effects of SiOx Barrier Layer Prepared by Plasma-Enhanced Chemical Vapor Deposition on Improvement of Long-Term Reliability and Production Cost for Cu-Plated Amorphous Si/Crystalline Si Heterojunction Solar Cells," *Solar Energy Materials & Solar Cells* 163 (2017): 204–209, https://doi.org/10.1016/j.solmat.2016.12.029.

27. J. Yu, Y. Bai, Q. Qiu, et al., "Reliability of Transparent Conductive Oxide in Ambient Acid and Implications for Silicon Solar Cells," *eScience* 4, no. 3 (2024): 100241, https://doi.org/10.1016/j.esci.2024.100241.

28. O. A. Arruti, A. Virtuani, and C. Ballif, "Long-Term Performance and Reliability of Silicon Heterojunction Solar Modules," *Progress in Photovoltaics: Research and Applications* 31, no. 7 (2023): 667–677, https://doi.org/10.1002/pip.3688.

29. S. Li, M. Pomaska, A. Lambertz, et al., "Transparent-Conductive-Oxide-Free Front Contacts for High-Efficiency Silicon Heterojunction Solar Cells," *Joule* 5, no. 6 (2021): 1535–1547, https://doi.org/10.1016/j.joule.

30. D. D. Tune, N. Mallik, H. Fornasier, and B. S. Flavel, "Breakthrough Carbon Nanotube-Silicon Heterojunction Solar Cells," *Advanced Energy Materials* 10, no. 1 (2020): 1903261, https://doi.org/10.1002/aenm.201903261.

31. G. Makrides, B. Zinsser, M. Norton, and G. E. Georghiou, *Third Generation Photovoltaics Chapter 9: Performance of Photovoltaics Under Actual Operating Conditions* (London, UK: IntechOpen Limited, 2012), https://doi.org/10.5772/27386.

32. V. Sharma, A. Kumar, O. S. Sastry, and S. S. Chandel, "Performance Assessment of Different Solar Photovoltaic Technologies Under Similar Outdoor Conditions," *Energy* 58, no. 1 (2013): 511–518, https://doi.org/10.1016/j.energy.2013.05.068.

33. Q. Tang, W. Duan, A. Lambertz, et al., "> 85% Indium Reduction for High-Efficiency Silicon Heterojunction Solar Cells With Aluminum-Doped Zinc Oxide Contacts," *Solar Energy Materials & Solar Cells* 251, no. 5 (2023): 112–120, https://doi.org/10.1016/j.solmat.2022.112120.

34. J. Hüpkes, J. I. Owen, M. Wimmer, et al., "Damp Heat Stable Doped Zinc Oxide Films," *Thin Solid Films* 555 (2014): 48–52, https://doi.org/10.1016/j.tsf.2013.08.011.

35. D. Greiner, S. E. Gledhill, C. Koeble, et al., "Damp Heat Stability of Al-Doped Zinc Oxide Films on Smooth and Rough Substrates," *Thin Solid Films* 520, no. 4 (2011): 1285–1290, https://doi.org/10.1016/j.tsf.2011.04.190.

36. A. B. Morales-Vilches, A. Cruz, S. Pingel, et al., "ITO-Free Silicon Heterojunction Solar Cells With ZnO:Al/SiO$_2$ Front Electrodes Reaching a Conversion Efficiency of 23%," *IEEE Journal of Photovoltaics* 9, no. 1 (2019): 34–39, https://doi.org/10.1109/JPHOTOV.2018.2873307.

37. W. Duan, A. Lambertz, K. Bittkau, et al., "A Route Towards High-Efficiency Silicon Heterojunction Solar Cells," *Progress in Photovoltaics: Research and Applications* 30, no. 4 (2021): 384–392, https://doi.org/10.1002/pip.3493.

38. International Electrotechnical Commission, *IEC 61215-2: Terrestrial Photovoltaic (PV) Modules-Design Qualification and Type Approval-Part 2: Test Procedures* (Geneva, Switzerland: International Electrotechnical Commission, 2021).

39. T. Potthoff, K. Bothe, U. Eitner, D. Hinken, and M. Köntges, "Detection of the Voltage Distribution in Photovoltaic Modules by Electroluminescence Imaging," *Progress in Photovoltaics: Research and Applications* 18, no. 2 (2010): 100–106, https://doi.org/10.1002/pip.941.

40. B. Li, A. Stokes, and D. M. J. Doble, "Evaluation of Two-Dimensional Electrical Properties of Photovoltaic Modules Using bias-Dependent Electroluminescence," *Progress in Photovoltaics: Research and Applications* 20, no. 8 (2012): 936–944, https://doi.org/10.1002/pip.1161.

41. J. Bauer, F. Felix, and O. Breitenstein, "Quantitative Local Current-Voltage Analysis and Calculation of Performance Parameters of Single Solar Cells in Modules," *Solar Energy Materials & Solar Cells* 159 (2017): 8–19, https://doi.org/10.1016/j.solmat.2016.08.029.

42. A. S. Rajput, J. W. Ho, Y. Zhang, S. Nalluri, and A. G. Aberle, "Quantitative Estimation of Electrical Performance Parameters of Individual Solar Cells in Silicon Photovoltaic Modules Using Electroluminescence Imaging," *Solar Energy* 173 (2018): 201–208, https://doi.org/10.1016/j.solener.2018.07.046.

43. D. B. Sulas, S. Johnston, and D. C. Jordan, "Comparison of Photovoltaic Module Luminescence Imaging Techniques: Assessing the Influence of Lateral Currents in High-Efficiency Device Structures," *Solar Energy Materials & Solar Cells* 192 (2019): 81–87, https://doi.org/10.1016/j.solmat.2018.12.022.

44. D. Qiu, W. Duan, A. Lambertz, et al., "Transparent Conductive Oxide Sputtering Damage on Contact Passivation in Silicon Heterojunction Solar Cells With Hydrogenated Nanocrystalline Silicon," *Solar RRL* 6, no. 10 (2022): 2200651, https://doi.org/10.1002/solr.202200651.

45. D. W. Lee, W. J. Cho, J. K. Song, et al., "Degradation Behaviors of EVA Encapsulant and AZO Films in Cu(In,Ga)Se$_2$ Photovoltaic Modules Under Accelerated Damp Heat Exposure," *Solar Energy Materials & Solar Cells* 136 (2015): 135–141, https://doi.org/10.1016/j.solmat.2014.12.036.

46. D. B. Sulas, S. Johnston, and D. C. Jordan, "Imaging Lateral Drift Kinetics to Understand Causes of Outdoor Degradation in Silicon Heterojunction Photovoltaic Modules," *Solar RRL* 3, no. 8 (2019): 1900102, https://doi.org/10.1002/solr.201900102.

Supporting Information

Additional supporting information can be found online in the Supporting Information section.